Phase Behavior and Formation Dynamics of Helically Wound Networks: Generalized Janus Chain Model

Y. Ding, and M. Kro#ger

Macromolecules, **2009**, 42 (3), 576-579 • DOI: 10.1021/ma802459w • Publication Date (Web): 07 January 2009

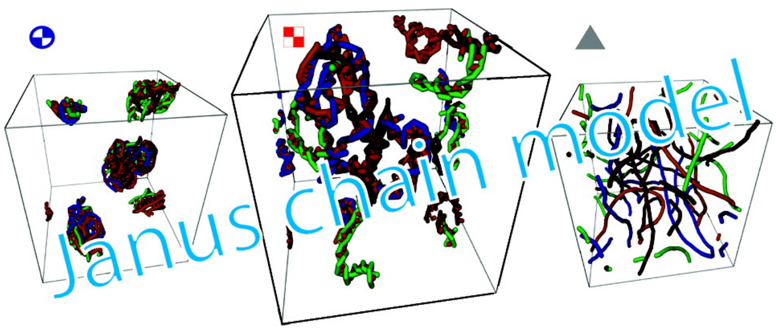

Phase Behavior and Formation Dynamics of Helically Wound Networks: Generalized Janus Chain Model

Y. Ding and M. Kröger*

Polymer Physics, Department of Materials and Materials Research Center, ETH Zurich, Wolfgang-Pauli-Str. 10, CH-8093 Zurich, Switzerland, and Computational Science, ETH Zurich, Universitätsstr. 6, CH-8092 Zurich, Switzerland

Received November 3, 2008
Revised Manuscript Received December 11, 2008

Physical properties of helical structures on the supramolecular level, such as observed in many physical and biophysical networks (collagen, dendronized polymers) and also the formation dynamics of such systems, are important areas of research. Approaches to their understanding and manipulation usually involve the self-assembly of chiral molecular building blocks,[1] where the "internal'' asymmetry of the building blocks is explicitly used. The more challenging question is on how to obtain helix formation in systems that do *not* contain any chiral centers. Evidence of such kind has been reported from both experiment[2] and theory.[3,4] The mechanism of helical formation had been attributed to local symmetry breaking. Here we propose a universal model for investigating formation and properties of helically interwound fibrous structures based on achiral systems. It is based on the so-called Janus chain (JC) model recently introduced by us and originally designed for high generation dendronized polymers[5] which consist of a number of dendrons attached to a linear polymeric backbone. The main idea behind the dynamical model is the observation that polarities are different for the chemical groups on the dendron termini and interior. This polarity difference allows to consider them as amphiphiles, which are known to give rise to a great variety of supramolecular assemblies.[6] Unlike conventional amphiphiles such as block copolymers, structurally more complicated dendronized polymers potentially exhibit a dynamical amphiphilic pattern on their solvent contacting interface.[4,7,8] The anisotropy related to the local symmetry breaking of amphiphilic pattern[4,8] is effectively captured by the JC model.

Apart from dendronized polymers, many helical fibrous structures are formed via amphiphilic self-assembly in solution (mostly water). Examples include actin filaments, DNA double strands, and collagen gels.[9,10] In this communication we stress the universality of the JC model and explore its range of applicability, which is seen to go beyond the case of double-helical dendronized polymer structures. Despite the fact that the formation mechanisms of helical superstructures are differing from case to case, and are sensitive to whether chiral or achiral building blocks are involved, the final superstructures possess structural and mechanical similarity. The JC model can be used to study dynamical properties of helical networks, with or without considering details of the formation process.

There are a number of simple mesoparticle models which capture the characteristics of gel-forming systems, such as irreversible gelation via sticky particle models[11] or more recent network formation models employing (i) two- and three-body interactions between beads, giving rise to directional bonds (cf. ref 12) and (ii) the simple elastic Lennard-Jones model exhibiting filamentous structures and a sol−gel transition.[13] None of these models have yet addressed the existence of the polymeric backbone present in real physical gels. It is worthwhile to mention that a system with purely radial interaction is prone to undergo a phase separation[14] and is therefore not a good model for a gel-forming system.[15]

Structurally simple polymers are usually modeled on the coarse-grained level by anharmonic multibead chains, where each linear chain consists of a number N of beads connected by anharmonic, finitely extendable nonlinear elastic (FENE) springs with bond vectors denoted as $\mathbf{b}_i$, bond length b_i. Semiflexibility is introduced by adding a bending Hamiltonian; excluded volume and solvent quality are taken into account by a radially symmetric Lennard-Jones potential between all beads.[16,17] The solvent is modeled either by explicit solvent particles or by Brownian dynamics, with or without hydrodynamic interactions.[18]

The JC model (see Figure 1) builds on a system of semiflexible excluded volume multibead FENE chains. The potential energy fully characterizing this system is a superposition of FENE, bending, and Lennard-Jones potential, more formally $U \equiv \sum_i U^{\mathrm{FENE}}(b_i) + U_i^{\mathrm{bend}} + \sum_j U^{\mathrm{LJ}}_{\chi_0}(r_{ij})$ with the classical ingredients[17] $U^{\mathrm{FENE}}(b) = -(k/2)b_0^2 \ln[1 - (b/b_{\max})^2]$ where $b_{\max}$ is the maximum extensibility of a bond, and bending potential $U_i^{\mathrm{bend}} = -\kappa \hat{\mathbf{b}}_i \cdot \hat{\mathbf{b}}_{i+1}$, where $\mathbf{r}_{ij}$ is the distance vector between beads i and j and the hat denotes the corresponding unit vectors. The $U^{\mathrm{LJ}}_{\chi_0}(r) = 4f(r)(r^{-12} - r^{-6} + {}^1/_4)$ contribution equals the classical Lennard-Jones potential truncated at distance r_c and modified by a prefactor which depends on distance: $f(r) = 1$ and $f(r) =$

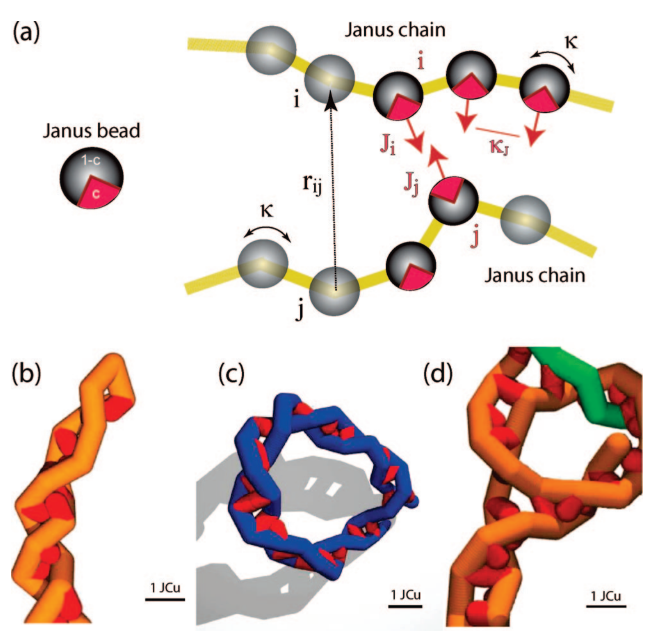

Figure 1. (a) Schematic representation of two semiflexible Janus chains approaching each other. Shown are the Janus beads interacting via radially symmetric LJ potentials, the bending coefficient κ, the distance vector $\mathbf{r}_{ij}$, two Janus vectors $\hat{\mathbf{J}}_i$ and $\hat{\mathbf{J}}_j$, and the fraction c of hydrophobic surface, interacting via the Janus−Janus potential (2a). (b−d) Characteristic types of polymeric conformations observed inside the helical network, where Janus vectors derive from nearest neighbor interactions ($\alpha = \infty$) and are drawn in red: (b) backfolded single polymer (solvent quality: $\chi_0 = -8$, $\Delta\chi = 32$, $c = 0.7$); (c) ring formation of a single polymer (−2, 32, 0.5); (d) cross-link point involving three chains (−4, 16, 0.7).

* Corresponding author. E-mail: mk@mat.ethz.ch.

10.1021/ma802459w CCC: $40.75
Published on Web 01/07/2009

χ_0 for $r \leq 2^{1/6}$ and $r \geq 2^{1/6}$, respectively. The attractive part of the LJ potential is weighted by χ_0, the solvent quality parameter.[17] Throughout this paper, units are reduced to LJ units, denoted as JCu for the present purpose.[19] For all results to be presented in this communication we have used $b_{\max} = 1.5$ and $\kappa = 25$. If not otherwise mentioned, $r_c = 1.275$, $k = 30$, and the bead number density is 5%.

Next, we add degrees of freedom to the classical FENE chain by introducing so-called JC unit vectors $\{\hat{\mathbf{J}}_i\}$ to each of the beads. A Janus vector characterizes the local anisotropy of an otherwise spherically symmetric bead. For amphiphilic systems, the Janus vector is considered as a dipole pointing from the hydrophilic center to the hydrophobic center. Within the generalized JC model to be introduced here, the Janus vector $\hat{\mathbf{J}}_i$ of bead i is induced by the surrounding of bead i, much in the spirit of embedded atom theories, where the induced quantity is usually a scalar (representing electron density) rather than a vector. To be specific, the orientation $\hat{\mathbf{J}}_i$ is given by a weighted sum over normalized connectors $\hat{\mathbf{r}}_{ij} \equiv \mathbf{r}_{ij}/r_{ij}$ between bead i and the spatially nearest nonbonded neighbors of bead i

$$\hat{\mathbf{J}}_i = \sum_j w(r_{ij})\ \mathbf{r}_{ij} \Big/ \sum_j w(r_{ij}) \tag{1}$$

with a finite-range weight function $w(r)$, which we choose as $w(r) = r^{-\alpha} - r_c^{-\alpha}$ with exponent α and cutoff distance r_c. The limiting cases $\alpha = 0$ and $\alpha \to \infty$, at large r_c, correspond to mean-field and nearest-neighbor weighting, respectively. The idea behind this simple treatment is that the hydrophobic and hydrophilic components are redistributed due to binary interactions and that the resulting pairs of mutually corresponding Janus vectors effectively prevent the further assembly (into aggregates). In the figures to be presented in this communication, such as Figure 1, besides the polymeric contour and beads, the massless Janus vectors will be drawn in red.

In an amphiphilic system, solvent shows different qualities to different components. For the case of an aqueous system, water acts as good (bad) solvent with respect to the hydrophilic (hydrophobic) components. Our model parameter $\Delta\chi \geq 0$, explicitly defined in the Janus–Janus interaction potential (2a), captures this difference on solvent qualities, while χ_0 acts as the midpoint solvent quality between the two extremes or, equally, the mean solvent quality of the two components. The isotropic LJ potential containing χ_0 quantifies the effect of solvent on nonlocal (global) interactions. The anisotropic part containing $\Delta\chi$ together with the Janus vectors describes the amphiphilic interaction $U^{\mathrm{J-J}}$ between Janus vectors $\mathbf{J}_i$ and $\mathbf{J}_j$ at bead–bead distance $\mathbf{r}_{ij}$:

$$\mathrm{U}_{ij*}^{\mathrm{J-J}} = \pm c(1 - c)\Delta\chi |g_{ij}g_{ji}| U_0^{\mathrm{LJ}}(r_{ij}) \tag{2a}$$

$$g_{ij} \equiv (\mathbf{J}_i \cdot \hat{\mathbf{r}}_{ij} - \cos c\pi)/(1 - \cos c\pi) \tag{2b}$$

where U_0^{LJ} is the purely attractive part of the LJ potential, and coverage $c \in [0, 1]$ is the fraction of hydrophobic components; it appears not only in the geometric factor g_{ij}, which derives from considering two conusoidally labeled objects (cf. Figure 1a) in contact, but also in the interaction strength, which must be symmetric with respect to the transformation $c \to 1 - c$ and which vanishes when either $c = 0$ or $c = 1$, i.e., in the case of a single component. The plus sign in (2a) applies when the geometric factors g_{ij} and g_{ji} are both positive; otherwise, the minus sign is in place. The asterisk in the subscript of $U_*^{\mathrm{J-J}}$ indicates that only nonbonded pairs of beads are subjected to this JC potential. Since our Janus vectors are instantaneously defined by the surrounding configuration, we implicitly regard the corresponding relaxation time for amphiphilicity redistribution to be much smaller than the configurational dynamics of the JC; i.e., we implicitly make use of time-scale separation underlying the multiscale approach. Still, according to their definition, the dynamics of Janus vectors is dictated by the configurational dynamics of surrounding chains.

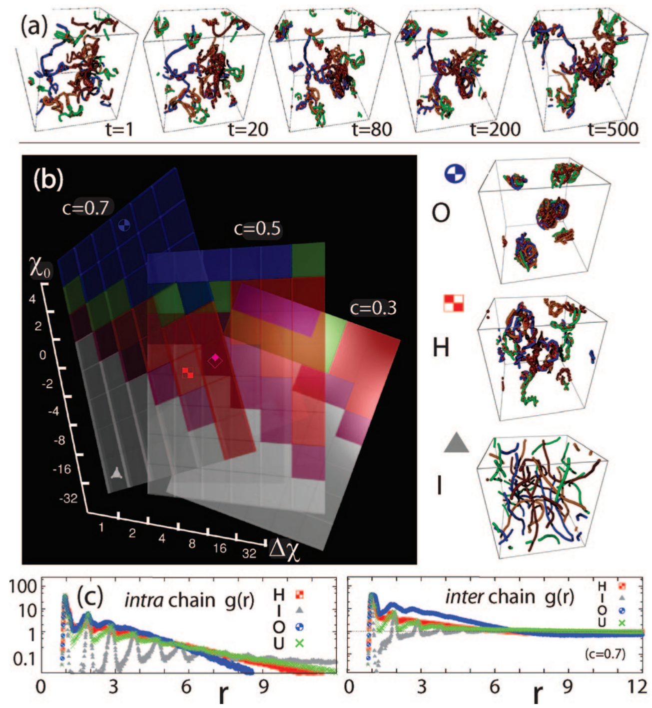

Figure 2. (a) Sample snapshots showing the formation of helical network, taken at times $t = 1$, 20, 80, 200, and 500 (Brownian dynamics simulation), for the case with solvent qualities $\chi_0 = -8$, $\Delta\chi = 16$, coverage $c = 0.7$, and nearest-neighbor interactions ($\alpha = \infty$). (b) Phase diagrams of JCs with coverages $c = 0.3$, 0.5 and 0.7 in the $\Delta\chi$–χ_0 plane. Gray stands for individual chains (I); light purple stands for the intermediate state (L) between individual chains (I) and helical network (H); bright red for helical network (H); green for the intermediate state (D) between helical network (H) and ball-like aggregate (O, blue). (right) Three representative configurations for (O) globules (solvent quality $\chi_0 = +4$, $\Delta\chi = 8$, coverage $c = 0.7$), (H) helical network (−8, 16, 0.7), and (I) individual chains. (−32, 1, 0.7). (c) Semilog plots of intra- and interchain pair correlation functions of JCs (here for coverage $c = 0.7$) are used to classify states into three representative phases (O, H, and I).

The Janus vectors represent the induced chemical asymmetry of a Janus bead, which is potentially pronounced for "thick" macromolecules with bulky side groups. The asymmetry, once realized, induces spontaneous curvature of the JC, in accord with a bending hamiltonian of the form $H \propto (\hat{\mathbf{J}} + \hat{\mathbf{b}}_{i-1} + \hat{\mathbf{b}}_i)^2$ as proposed in ref 4. In view of the part absorbed by the above bending potential (involving κ) this effect is captured by the following additional intramolecular interaction

$$U_i^{\mathrm{J-J,bend}} = -\kappa_J\, \hat{\mathbf{J}}_i \cdot (\hat{\mathbf{b}}_i - \hat{\mathbf{b}}_{i-1}) \tag{3}$$

where κ_J expresses the strength of bending induced by Janus vectors. For results explicitly shown in this paper $\kappa_J = \kappa$. At this point one may ask how to choose or obtain the parameters of the generalized JC model which serve to study a real system. The parameters b_0, $b_{\max}$, and bending stiffness κ characterizing the structureless polymer ($\Delta\chi = 0$) result from the architecture of the polymeric backbone, length of spacers between monomers, and, for dendronized polymers, the generation-sensitive persistence length and thickness of the polymer. The latter two

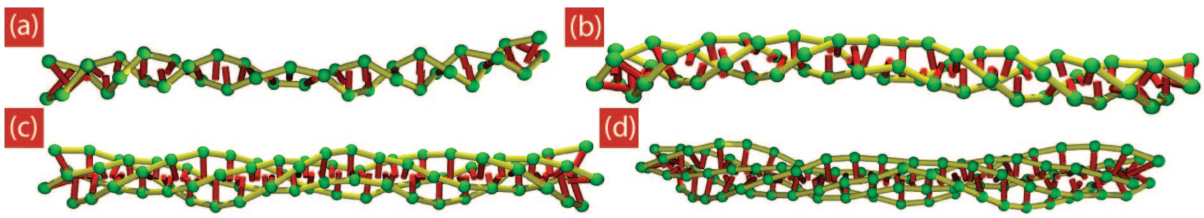

Figure 3. Shown are examples for (a) double helix at coverage $c = 0.35$ and $\alpha = 12$, (b) triple ($c = 0.4$, $\alpha = 2$), (c) quadruple ($c = 0.8$, $\alpha = 2$), and (d) quintuple helix ($c = 0.9$, $\alpha = 2$). Remaining simulation parameters are $k = 15$, $\chi_0 = 1$, $\Delta\chi = 32$, and $r_c = 2$. Interaction-mediating, induced spontaneous Janus vectors are drawn in red. The network formation dynamics of a system exhibiting double-helical structures to a large extent is animated in Figure 4a–e. For a gel formed by triple-helical structures see Figure 4f–k. Movies available online at ref 21.

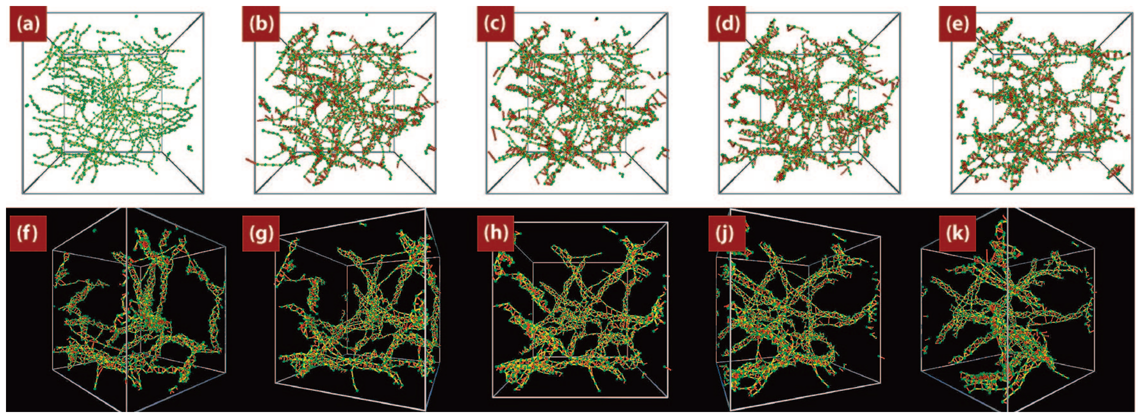

Figure 4. Sample snapshots for systems mentioned in Table 1 taken (a–e) during the formation dynamics of the double-helical network at coverage $c = 0.4$, $\alpha = 12$, and (f–k) during the static rotation of a triple-helical network in its stationary state at $c = 0.6$, $\alpha = 12$. Remaining simulation parameters are $\chi_0 = 1$, $\Delta\chi = 32$, and $r_c = 2$. The time passed between snapshots (a) and (e) is 10 JC units. Movies available online at ref 21.

quantities can be estimated using a simple Flory-type approach, as done for dendrimers in ref 20, where the spherical volume in the interaction term is replaced by a cylindrical one. While χ_0 has been related to solvent quality, the coverage c is determined by the given chemistry. More precisely, it should be related to the functionality of junctions inside dendronized polymer. While a bottlebrush with one or a few terminal monomers per strand will be characterized by $c \ll 1$, a copolymer brush or dendronized polymer may be well characterized by large values for $0 \ll c < 1$. For the DPs with three-functional junctions of refs 4, 5, and 13, for example, approximately half of the monomers are hydrophilic. There is a route to estimate these parameters using atomistic simulation.[4] By inspecting the energies, we see that $\Delta\chi$ quantifies the strength of Janus–Janus interaction and α the range of interaction between Janus beads, while κ_J quantifies the tendency of the molecule to bend as a result of redistribution of hydrophobic and hydrophilic components. A large $\kappa_J \gg \kappa$ will therefore favor formation of compact helices while a weak $\kappa_J \ll \kappa$ will allow formation of gently bent multiple bundles. However, as this approach cannot be successfully followed for complex molecules like DP in view of today's computational possibilities, and because it would limit our presentation to a particular system, we here present the reverse strategy, and investigate the effect of model parameters χ_0, $\Delta\chi$, and c on the phase behavior.

By now, the force $\mathbf{F}_i = -\partial E/\partial \mathbf{r}_i$ on particle i is immediately obtained from the model energy $E = U + U^{\mathrm{J-J}} + U^{\mathrm{J-J,bend}}$. We refrain from writing down the full expression, but mention the useful identity $\partial\hat{\mathbf{b}}_k/\partial\mathbf{r}_i = b_k^{-1}(\delta_{i,k+1} - \delta_{i,k})(\mathbf{1} - \hat{\mathbf{b}}_k\hat{\mathbf{b}}_k)$, where δ is the Kronecker symbol, $\mathbf{1}$ the unity matrix, and $\hat{\mathbf{b}}_k\hat{\mathbf{b}}_k$ a dyadic product. We apply conventional Brownian dynamics as described in textbooks[17,18] to study the Langevin equation for the JC model. The equations of motion for a number of these chains (according to given concentration) confined in a cubic simulation cell are solved subject to periodic boundary conditions.

Before we turn to structural properties of the many-chain system and the phase diagrams, let us inspect typical single chain conformations formed inside the system made of a large number of JCs. Three of them are shown in Figure 1b–d. All chains shown in this figure are found in a helical conformation, which results from the Janus–Janus interaction. Figure 1b shows a backfolding helical chain, which can be observed if the energy penalty for the kink (due to the stiffness κ) is smaller than the energy gain stemming from amphiphilic Janus–Janus interactions in the backfolded part of the chain. Similarly, linear chains can aggregate into rings when their length over stiffness ratio and concentration are both small enough to give the hydrophobic interaction the possibility to become active and to create a metastable physical bond between chain ends or, more generally, between parts of the same chain. Rings are formed in a two-step process. After touching and formation of temporary junctions, bending energy is lowered by lateral motion of junction toward the chain ends. At the same time, the chain tends to lower the Janus–Janus bending energy (3) which favors formation of helical chains with constant pitch.

A 3D phase diagram obtained from 144 simulations upon varying coverage c and solvent quality parameters χ_0 and $\Delta\chi$ is presented in Figure 2b. Snapshots showing formation of helical network are shown in Figure 2a. Isocoverage surfaces at $c =$ 0.3, 0.5, and 0.7 leave a good impression about the whole phase diagram of JC systems in the $\Delta\chi$–χ_0 plane. By analyzing the inter- and intramolecular pair correlation functions (example given in Figure 2c) and also visual inspection, we have classified all states into three main regimes: individual noncollapsed chains (phase I), helical network (H), and individual ball-like globules (O). Three representative and accordingly labeled configurations

Table 1. Overview about the Effect of Interaction Quality (α) and Coverage (c) on the Appearance of Multihelical Structures as the Ones Shown in Figures 3 and 4 ($\chi_0 = 1$, $\Delta\chi = 32$, $r_c = 2$)[a]

	$c = 0.35$	$c = 0.4$	$c = 0.6$	$c = 0.8$
$\alpha = 2$	triple	triple	quadruple	quintuple
$\alpha = 12$	double	triple	quadruple	quintuple
$\alpha = \infty$	double	double	irregular double	globule

[a] Parameter α influences the phase behavior only at low coverages as it mainly influences the orientation of Janus vectors (Janus vectors point to the average direction constructed from neighboring beads and to the closest neighbor for small and large α values, respectively). At high coverages c, the orientation of the Janus vector plays a minor role. The case $\alpha = \infty$ has been discussed in more detail; cf. Figure 2.

characterizing the three main phases are shown on the right part of Figure 2. Notice that these results have been obtained for a limiting case of our model, the one where the Janus vectors are determined by nearest-neighbor segments ($\alpha = \infty$). Under this original setting of the JC model, we find that double-helical network formation is favored over multihelical agglomeration. The latter we do not observe for range of parameters used to study phase diagrams in Figure 2b.

However, as we will demonstrate next, the presented model is well capable of capturing the dynamics and physics of more complex phases. A pertinent example elucidating the range of applicability of the same model is offered next. We have varied the range of interaction, captured by parameter α of our model. While $\alpha = \infty$ corresponds to a maximally short-range interaction, smaller powers α allow parts of the chains to interact not only with their nearest neighbor but with surrounding material in second- and higher-order shells. The double-helical chain is essentially stable due to the short-range interaction chosen in the previous examples as it effectively repulses any additional chain approaching the formed cluster. By probing finite values for α, we are able to observe multihelical structures, as demonstrated in Figure 3. As is evident from these snapshots, there is a tendency to form ideal multihelices in the absence of surrounding chains, i.e., at low concentrations. Upon increasing concentration, the systems starts to gel. The qualitative behavior is summarized in Table 1, corresponding time series and snapshots given in Figure 4. We observe formation of infinite clusters whose mesh characteristics are apparently unaffected by system size as soon as it exceeds 3−4 times the size of typical spacers between junctions.

Modeling of the mechanical properties of filamentous protein networks[9] has attracted noticeable attention.[22] We have evidence that the intrinsic stiffness of bundles increases with the order of helicity and that their effect on mesoscopic structures largely affects the material behavior, mesh size, and other properties of the samples. To this end, we subjected the equilibrated JC systems to shear and elongational deformation (or flow) by applying methods presented elsewhere.[17,23] In particular, for the double-helical JC network we find (i) a high shear modulus (comparable with the one for a polymer melt of same concentration), (ii) strain hardening, and (iii) negative normal stresses when sheared, in agreement with experimental findings of real biopolymer networks.[24] The dynamics of the network formation process, the process of chain interwinding, and formation of multihelices has been animated and is permanently available online at ref 21, where we have summarized supporting information movies, in particular.

To summarize, we have presented results for the phase behavior, formation dynamics, and structure of the JC model. The generalized JC model seems to contain a sufficient, but minimum, amount of ingredients to capture the internal structure of bulky, linear polymers (large side groups, achiral building blocks such as it is the case for dendronized polymers and other multihelical bundles). We are not aware of the existence of an alternate, competitive coarse-grained model of such 3D semiflexible polymer networks. The generalized JC model should be of use for the study of material properties of biopolymer networks made of chiral building blocks, too. The time and length scales[19] reachable by the presented model, when combined with atomistic simulation of specific chemistry (as exemplified in[4] for the unmodified JC model) in order to estimate model parameters, may help to study the dynamics of network formation and material properties efficiently.

References and Notes

(1) Jahnke, E.; et al. *Adv. Mater.* **2008**, *20*, 409. Yuan, J.; et al. *J. Org. Chem.* **2006**, *71*, 5457.
(2) Böttcher, C.; et al. *Chem.—Eur. J.* **2005**, *11*, 2923. Percec, V.; et al. *Nature (London)* **2002**, *419*, 384. Zhuang, W.; et al. *Adv. Mater.* **2008**, *20*, 3204.
(3) Christopoulos, D. K.; et al. *J. Chem. Phys.* **2006**, *125*, 204907.
(4) Ding, Y.; et al. *J. Chem. Phys.* **2007**, *127*, 094904.
(5) Schlüter, A. D.; Rabe, J. P. *Angew. Chem., Int. Ed.* **2000**, *39*, 864. Frauenrath, H. *Prog. Polym. Sci.* **2005**, *30*, 325.
(6) Ringsdorf, H.; et al. *Angew. Chem., Int. Ed. Engl.* **1988**, *27*, 113. Förster, S.; Antonietti, M.; et al. *Adv. Mater.* **1998**, *10*, 195.
(7) Giupponi, G.; Buzza, D. M. A. *J. Chem. Phys.* **2004**, *120*, 10290.
(8) Ding, Y.; Kröger, J. *J. Comput. Theor. Nanosci.* **2009**, in press.
(9) Lieleg, O.; et al. *Phys. Rev. Lett.* **2007**, *99*, 088102.
(10) Storm, C.; et al. *Nature (London)* **2005**, *435*, 191. van der Heijden, G.; Horton, M.; et al. *Biophys. J.* **2007**, *92*, 70.
(11) De Michele, C.; et al. *J. Phys. Chem. B* **2006**, *110*, 8064. Corezzi, S.; et al. *Soft Matter* **2008**, *4*, 1173.
(12) Del Gado, E.; Kob, W. *Phys. Rev. Lett.* **2007**, *98*, 028303. Del Gado, E.; Kob, W. *J. Non-Newtonian Fluid Mech.* **2008**, *149*, 28.
(13) Peleg, O.; et al. *Europhys. Lett.* **2007**, *77*, 58007. Kröger, M.; et al. *Soft Matter* **2008**, *4*, 18. Peleg, O.; et al. *Macromolecules* **2008**, *41*, 3267.
(14) Puertas, A.M.; et al. *J. Chem. Phys.* **2004**, *121*, 2813.
(15) A model which shares technical similarity with the one presented in this work and may be recovered as special case is the FENE−CB model for wormlike micelles[25] and semiflexible equilibrium polymers. Strong ferrofluids exhibit the formation of transient polymeric chains[26] but do not gel. To our knowledge, helical structures have not been observed for the two mentioned classes of achiral systems, presumably due to the lack of complex internal structure of their constituents.
(16) Del Gado, E.; Kob, W. *Europhys. Lett.* **2005**, *72*, 1032.
(17) Kröger, M. *Models for Polymeric and Anisotropic Liquids*; Springer: Berlin, 2005. Kröger, M. *Phys. Rep.* **2004**, *390*, 453. Kröger, M.; et al. *J. Rheol.* **1993**, *37*, 1057.
(18) Öttinger, H. C. *Stochastic Processes in Polymeric Fluids*; Springer: Berlin, 1996. Jendrejack, R. M.; et al. *J. Chem. Phys.* **2000**, *113*, 2894. Kröger, M.; et al. *J. Chem. Phys.* **2000**, *113*, 4767.
(19) Reduced units−online interactive tool: http://www.complexfluids.ethz.ch/units.
(20) Boris, D.; Rubinstein, M. *Macromolecules* **1996**, *29*, 7251.
(21) Addon material for this article permanently available at : http://www.complexfluids.ethz.ch/JC.
(22) Head, D. A.; et al. *Phys. Rev. Lett.* **2003**, *91*, 108102. Wilhelm, J.; Frey, E. *Phys. Rev. Lett.* **2003**, *91*, 108103. Huisman, E. M.; et al. *Phys. Rev. Lett.* **2007**, *99*, 208103.
(23) Todd, B. D.; Daivis, P. J.; et al. *Phys. Rev. Lett.* **1998**, *81*, 1118. Hess, S. *Physica A* **1997**, *239*, 449. Kim, J. M.; et al. *J. Non-Newtonian Fluid Mech.* **2007**, *152*, 168.
(24) Wen, Q.; et al. *New J. Phys.* **2007**, *9*, 428.
(25) Carl, W.; et al. *J. Phys. II* **1997**, *7*, 931. Kröger, M.; Makhloufi, R. *Phys. Rev. E* **1996**, *53*, 2531. Briels, W. J.; et al. *J. Phys.: Condens. Matter* **2004**, *16*, S3965.
(26) Zubarev, A. Y.; et al. *J. Magn. Magn. Mater.* **2002**, *252*, 241. Ilg, P.; Kröger, M. *Phys. Rev. E* **2002**, *66*, 021501. Kröger, M.; et al. *J. Phys.: Condens. Matter* **2003**, *15*, S1403.

MA802459W